Unraveling the Hydrogen Bond Network in a Theophylline-Pyridoxine Salt Cocrystal by a Combined X-ray Diffraction, Solid-State NMR, and Computational Approach

UNRAVELING THE HYDROGEN BOND NETWORK IN A THEOPHYLLINE-PYRIDOXINE SALT COCRYSTAL BY A COMBINED X-RAY DIFFRACTION, SOLID-STATE NMR AND COMPUTATIONAL APPROACH

Federica Rossi,[1] Paolo Cerreia Vioglio,[2] Simone Bordignon,[1] Valeria Giorgio,[1] Carlo Nervi,[1] Emanuele Priola,[1] Roberto Gobetto,[1] Koji Yazawa,[3] Michele R. Chierotti[1]*

[1] Department of Chemistry and NIS Centre, Università di Torino, Via P. Giuria 7, 10125 Torino, Italy
[2] present address Aix-Marseille Université, CNRS, ICR (UMR 7273), 13013 Marseille, France
[3] JEOL RESONANCE Inc., Akishima, Tokyo 196-8558, Japan

Abstract

The formation of a codrug, a cocrystal formed by two active pharmaceutical ingredients (APIs), between theophylline (THEO) and pyridoxine·HCl ($PyrH^+Cl^-$) is reported. The THEO $PyrH^+Cl^-$ drug-drug cocrystal could turn out to be interesting in the pharmaceutical field because these two APIs are concurrently administered for asthma treatment. The codrug was characterized by a combined experimental and computational investigation by means of SCXRD, SSNMR and DFT calculations. An exhaustive SSNMR study was performed to unravel the complex network of hydrogen bond interactions which was poorly defined by SCXRD. Several advanced 2D SSNMR spectra such as ^{1}H DQ MAS, ^{13}C-^{1}H HETCOR, ^{14}N-^{1}H J- and D-HMQC were acquired, taking advantage of the resolution and sensitivity improvement provided by indirect detection pulse sequences and very fast MAS at 70 kHz. These experiments, supported and completed by DFT calculations, were fundamental in accurately determining the position of hydrogen atoms and thus in elucidating the hydrogen bond network. They also allowed to define the ionic character of the drug-drug cocrystal, which can be more properly defined as a drug-drug salt cocrystal.

Introduction

The combination of multiple active pharmaceutical ingredients (APIs) into unit doses has become a popular strategy in particular for the therapy of many complex disorders, such as infectious diseases, HIV/AIDS, cancer, diabetes, and cardiovascular diseases.[1] This approach proves advantageous mainly for two reasons: (i) because monotherapy (i.e. targeting a specific receptor) is no longer considered effective, and (ii) because it results in reducing the pill load and also any possible mistake by patients, which often leads to high costs. When the necessity of taking more than one drug arises, which is frequent, indeed, for prolonged and elaborate therapies, complicated schedules for assumptions and doses are involved. It has been calculated that every year the consequences of a wrong approach to a therapy cost several billions of dollars, because of a quite large number of hospitalizations and deaths.[2,3]

Drug-drug cocrystallization is an alternative method to the employment of heterogeneous mixtures which could offer potential advantages over traditional combination drugs. Thanks to the supramolecular synthon approach, a codrug may also lead to an improvement, at least for one component, of physicochemical properties, such as enhanced solubility, dissolution rate and bioavailability,[4–6] chemical and physical stabilization through intermolecular interactions,[7,8] and assistance in lifecycle management of existing products. Furthermore, the possibility of patenting a codrug is significantly appealing for pharmaceutical companies from the intellectual property protection point-of-view.

Several codrugs can be found in the literature,[9] despite their complexity in design and synthesis. Some notable examples are those of theophylline with sulfamethazine,[7] barbital,[10] and 5-fluorouracil,[11] ethenzamide with gentisic acid,[12] and lamivudine with zidovudine.[13] Some of us recently reported on the obtainment of a codrug between indomethacin and caffeine that resulted in a 3 times improvement of the *in vitro* bioavailability of indomethacin,[14] suggesting that sometimes drug-drug cocrystallization represents a strategy to tune the performances of APIs. The recent approval by the US Food and Drug Administration (FDA) of the first drug-drug (sacubitril/valsartan) cocrystal product (Entresto, manufactured by Novartis) may spark even more interest in exploring new drug-drug cocrystal combinations.[15,16]

Theophylline (THEO) is a BCS (Biopharmaceutical Classification System) class I drug (high solubility, high permeability)[17–19] widely used as a bronchodilating agent for asthma treatment. However, it may produce serious side effects and its induced seizures lead to high morbidity and mortality.[20] Concerns regarding the risk-benefit ratio have resulted in its infrequent prescribing. Since the administration of THEO causes vitamin

B6 deficiency,[21] the side effects of its use can be reduced by prescribing vitamin B6, also known as pyridoxine (Pyr).[22,23] Thus, a codrug between THEO and Pyr or $PyrH^+Cl^-$ could prove valuable for the treatment of asthma, as well as from a crystal engineering point-of-view, because THEO possesses three hydrogen bond (HB) acceptors, two carboxylic moieties and a heterocyclic nitrogen atom, while $PyrH^+Cl^-$ displays several hydroxyl groups acting as HB donors (Scheme 1).

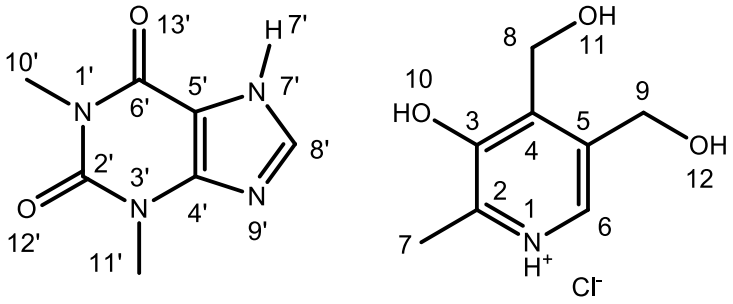

THEO $PyrH^+Cl^-$

Scheme 1. Chemical structures of THEO and $PyrH^+Cl^-$, with atom numbering.

THEO exists in four polymorphic forms[24–27] and two hydrates.[28,29] Recently, several codrugs were also reported with 5-fluorouracil,[11] phenobarbital,[10] diflunisal and diclofenac,[30] and sulfamethazine[7] In all these structures, N7' and N9' are always involved in strong HBs as donor and acceptor groups, respectively; the C6'=O13' moiety acts only rarely as a strong HB acceptor, while C2'=O12' forms almost always weak HBs with CH groups. On the other hand, $PyrH^+Cl^-$ exists as a single polymorph and, to the best of our knowledge, no codrugs involving it are present in the literature.

We report here on the preparation of a THEO·$PyrH^+Cl^-$ codrug formed by two APIs usually given in co-therapy. Moreover, the codrug represents a challenging model system from the HB characterization point-of-view, since several HB donors and acceptors (3 OH and 2 NH groups and 2 C=O moieties and 1 aromatic nitrogen atom) are present. The codrug was characterized by single crystal X-ray diffraction (SCXRD); however, owing to the poor definition of the hydrogen atom positions, a combined experimental and computational investigation by means of solid-state NMR (SSNMR) and DFT (density functional theory) calculations was performed to give a full and consistent description of the obtained drug-drug cocrystal. Due to its varied HB motifs, THEO·$PyrH^+Cl^-$ codrug offers a chance to test the limits of 1D and 2D SSNMR experiments in providing a complete assignment of strongly overlapped ^1H resonances associated to H-bonded atoms whose chemical shift is far from the "conventional" HB region (> 10 ppm). Several advanced 2D SSNMR spectra such as ^1H DQ MAS, ^{13}C-^1H HETCOR, ^{14}N-^1H J- and D-HMQC allowed to unravel the complex network of HB interactions (not fully clear from SCXRD data) and to define the ionic character of the drug-drug cocrystal which can be more properly defined as a drug-drug salt cocrystal. It is well known that SSNMR is able to provide information on HBs such as: detection and strength, from ^1H chemical shifts in 1D spectra[31–34], position of the hydrogen atom from ^{13}C and ^{15}N chemical shifts[35,36] and ^1H-^1H and ^1H-^{13}C spatial proximities, from 2D spectra.[37–39]

In the last years, advanced 2D experiments, leveraging the improved resolution achieved with sample spinning speeds higher than 70 kHz, have provided direct evidence of the position of the hydrogen atom along N···H···O contacts.[40] In particular, the ^1H-^{14}N HMQC experiment, applied both in the J- and in the D-version, offers insights on the formation of N-H···O rather than N···H-O interactions. The pulse sequence exploits the indirect detection of ^{14}N lineshapes through a combination of J-coupling and residual dipolar splittings (RDS) in the J-version,[41,42] whereas the D-version is based on the recoupling of ^1H-^{14}N heteronuclear dipolar interactions.[43–45]

Raman spectroscopy and thermal analyses (DSC and TGA) completed the characterization.

Experimental Part

THEO, hexane and ethanol were purchased from Sigma Aldrich, whereas $PyrH^+Cl^-$ from Alfa Aesar. All compounds and solvents were used without any further purification. THEO was verified to be in its form II by comparing experimental and calculated PXRD (data not shown) and the ^{13}C CPMAS SSNMR spectrum with those previously reported.[26,46]

White microcrystalline powder of THEO·PyrH$^+$Cl$^-$ was obtained by evaporating an ethanol solution of THEO (26 mg, 1.46*10^{-4} mol) and PyrH$^+$Cl$^-$ (30 mg, 1.46*10^{-4} mol) at room temperature. Sonication of the solution for 60 min before crystallization resulted essential for the achievement of the codrug. Plate-like single crystals for SCXRD were obtained by vapor diffusion crystallization: a 1:1 solution of THEO and PyrH$^+$Cl$^-$ in ethanol was exposed to hexane vapors for 7 days.

X-ray diffraction

The single-crystal data were collected with a Gemini R Ultra diffractometer with graphite-monochromated Mo-*K*α radiation (*λ* = 0.71073 nm) by the *ω*-scan method. The cell parameters were retrieved with the CrysAlisPro software and the same program was used to perform data reduction with corrections for Lorenz and polarizing effects. Scaling and absorption corrections were applied through the CrysAlisPro[47] multiscan technique. The structure of THEO·PyrH$^+$Cl$^-$ was solved with direct methods by using SHELXS-97[48] and refined with full-matrix least-squares techniques on *F*2 with SHELXL-97. All non-hydrogen atoms were refined anisotropically. Hydrogen atoms were located in the final Fourier difference maps and refined with coordinates and *U*iso calculated and riding on the corresponding bonded atoms. The bond lengths and angles are reported in Table S1 in the Supporting Information, and the crystal data and refinement results can be found in Table 1. The underlying net derived by simplification from the crystal structure was analyzed and represented with ToposPro, Version 5.1.0.9[49] by considering the HBs between different fragments as defining interactions.[50] The graphics of the crystal structure were generated using Mercury 3.9.[51] CCDC 1581747 contains the supplementary crystallographic data for THEO·PyrH$^+$Cl$^-$.

Table 1. THEO·PyrH$^+$Cl$^-$ crystal data.

Chemical formula	$C_7H_8N_4O_2$,$C_8H_{12}NO_3$,Cl
M_r	385.81
Crystal system, space group	Orthorhombic, *Pnma*
Temperature (K)	293
a, *b*, *c* (Å)	27.733(2), 6.6137(7), 9.0489(6)
V (Å^3)	1659.7(2)
Z	4
Radiation type	Mo *K*α
μ (mm^{-1})	0.271
Crystal size (mm^3)	0.73× 0.42× 0.36
T_{min}, T_{max}	0.85592, 1.000
No. of measured, independent and observed [$I > 2\sigma(I)$] reflections	6392, 5134, 1591
R_{int}	0.0543
$R[F^2 > 2\sigma(F^2)]$, $wR(F^2)$, S	0.0464, 0.0962, 1.065
No. of reflections	1591
No. of parameters	174
$\Delta\rho_{max}$, $\Delta\rho_{min}$ (e Å^{-3})	0.192, -0.276

Raman spectroscopy

Raman spectra were collected on a Bruker Vertex 70 instrument, equipped with a RAM II module. The employed excitation source was a 1064 nm laser with a power varying in the range 35-50 mW and a number of scans between 80 and 1000, depending on the sample; resolution was set at 4 cm^{-1} for all spectra. A spectral range of 50-4500 cm^{-1} was scanned, using a CaF_2 beam splitter. The spectra were processed with Bruker OPUS v.7.0 software. Raman spectroscopy was exclusively used for the cocrystallization screening.

Solid-state NMR measurements

^{13}C CPMAS and ^{15}N CPMAS 1D solid-state NMR measurements were performed on a Bruker Avance II 400 instrument operating at 400.2, 100.6 and 40.5 MHz for ^{1}H, ^{13}C and ^{15}N nuclei, respectively. Cylindrical 4 mm o.d. zirconia rotors with a sample volume of 80 μL were employed and spun at 12 (^{13}C) and 9 (^{15}N) kHz. ^{13}C and ^{15}N chemical shift scales were referenced to α-glycine (^{13}C methylene signal at 43.5 ppm),[52] and to

$(NH_4)_2SO_4$ (^{14}N signal at 0 ppm and ^{15}N signal at 24.7 ppm with respect to NH_3), respectively. Additional details about the chemical shift referencing may be found in the Supplementary Material.

^1H MAS, ^1H DQ MAS, 2D ^{13}C-^1H HETCOR (indirect detection), and 2D ^{14}N-^1H J- and D-HMQC (indirect detection) spectra were collected on a Jeol ECZR 600 instrument, operating at a frequency of 600.1, 150.9, and 43.4 MHz for ^1H, ^{13}C, and ^{14}N, respectively. Samples were packed in 1 mm (o.d.) cylindrical zirconia rotors (sample volume 0.8 μl). All measurements were acquired at probe temperature with a spinning speed of 70 kHz. Previous internal tests showed that, at 70 kHz, the sample temperature increase is about 20-25 Celsius degrees which is far below any possible conversion/melting/degradation point. Detailed information on the used pulse sequences and parameters is reported in the Supporting Information.

^1H, ^{13}C and ^{14}N chemical shift scales were referenced to the resonance of adamantane (^1H signal at 1.87 ppm), alanine (^{13}C methyl signal at 19.6 ppm),[53] $(NH_4)_2SO_4$ (^{14}N signal at 0 ppm with respect to NH_3), which were used as external standards.

Thermal analysis

Thermogravimetric analyses (TGA) were performed on a Q600 SDT TA instrument equipped with a DSC heat flow analyzer, using a temperature range of 40-400°C under 50 mL·min^{-1} N_2 flow. Samples (5-10 mg of weight) were placed into the furnace inside alumina crucibles and heated with a ramp of 10 °C·min^{-1}. Calorimetric experiments (DSC) were collected on a DSC Q200 TA instrument. Samples were accurately weighed (5-10 mg) and put into aluminium pierced pans. Calibration for temperature and heat flow was performed in a 40-350 °C temperature range, with heating rates of 10 °C·min^{-1}.

Computations

Periodic lattice calculations were performed by means of Quantum Espresso v.5.1.2.[54] The Generalized Gradient Approximation (GGA) functional PW86PBE[55] with the inclusion of the exchange-hole dipole moment (XDM)[56] dispersion correction method for accurate model of the HB interaction was used in all calculations. XDM dispersion energies were computed using the modified version of Quantum Espresso, adopting the appropriate damping parameters for the functional PW86PBE (a1 = 0.6836 and a2 = 1.5045). For geometry optimizations, the solid-state crystal structures were considered as starting structures. Calculations were performed with a fixed cell scheme by relaxing all atoms, adopting the Kresse-Joubert Projected Augmented Wave pseudopotentials.[57] A cut-off of 60 Ry was used for structural optimization, whereas NMR chemical shifts were calculated using an 80 Ry energy cut-off by the GIPAW method.[58] The Brillouin zones were automatically sampled with the Monkhorst-Pack scheme.[59] Geometry optimization and NMR chemical shift calculations were performed with a grid mesh of 1x2x2. The theoretical absolute ^1H, ^{13}C and ^{15}N magnetic shielding (σ) values were converted into the corresponding chemical shifts (δ) relative to the absolute magnetic shielding of the reference substance diazabicyclo[2:2:2]octane (dabco), computed at the same level. For practical purposes, the ^1H and ^{13}C chemical shifts were reported against TMS (the experimental values of δ ^1H and ^{13}C for dabco vs. TMS are 2.5 and 47.7 ppm, respectively); ^{15}N chemical shifts were reported against liquid ammonia (the experimental values of δ ^{15}N for dabco vs. liquid NH_3 is 10.9 ppm) in a similar way as previously described.[37]

Results and Discussion

Cocrystallization of equimolar quantities of THEO and $PyrH^+Cl^-$ in ethanol allowed to obtain the drug-drug cocrystal THEO·$PyrH^+Cl^-$. All the analytical techniques used, i.e., Raman, PXRD, and SSNMR show the quantitative formation of a new phase through remarkable changes in the spectral features (see Raman spectra and PXRD patterns in Figures S1 and S2 in the Supporting Information, respectively and ^{13}C CPMAS spectra in Figure 2). SCXRD provided the structure while SSNMR verified the formation of a drug-drug salt cocrystal and clarified the positioning of the H10, i.e. whether pointing toward N9' or O11. The comparison between the experimental and computed PXRD patterns (Figure S3 in the Supporting Information) confirms that the crystal structure is representative of the whole powder.

THEO·$PyrH^+Cl^-$ crystallizes in the orthorhombic space group *Pnma*. Accordingly to X-ray data and both ^{13}C and ^{15}N CPMAS NMR spectra (see below), the asymmetric unit (Figure S4 in the Supporting Information) contains one THEO and one $PyrH^+Cl^-$ molecule. Several SSNMR data (see below) agree with the preservation of the ionic character of $PyrH^+Cl^-$ in the cocrystal. The two molecular fragments are connected by a O11-H11···O12'^{I} HB (O11···O12'^{I} distance = 2.703(5) Å, I = x, y, z-1) (Figure 1a). On the other hand, the uncertainty in the

position of the H10 hydrogen atom does not allow to reveal if it points toward N9' to form an intermolecular O10-H10···N9' contact or toward O11 to form an intramolecular O10-H10···O11 HB. An in-depth SSNMR and DFT analysis (see below) shows that the intramolecular HB between the two vicinal alcoholic groups is present (O10···O11 distance = 2.554(5) Å). Thus, the proximity between N9' and O10 is due to the packing and it is perhaps favored by the C8'-H8'···O12'^{I} weak interaction (C8'···O12'^{I} distance = 3.593(4) Å; H8'···O12'^{I} distance= 2.399 Å, I = x, y, z-1; latter data obtained from the DFT optimized structure, see below). In this context, the C2'=O12' acts as a bifurcated HB acceptor with C2'=O12'···H8' and C2'=O12'···H11 angles of 142.4° and 149.6°, respectively in agreement with the most recurring values reported in the literature.[60] The molecules form layers through a complex network of HB interactions which involves the Cl^- ion (Figure 1c): N7'-H7'···Cl1^{-II} (N7'···Cl1^{-II} distance = 3.144(3) Å, II = ½+x, ½-y, ½ -z), O12^{III}-H12^{III}···Cl1$^-$ (O12^{III}···Cl1$^-$ distance = 3.145(4) Å, III = x-1, y, z-1) and N1^{+IV}-H1^{IV}···Cl1$^-$ (N1^{+IV}···Cl$^-$ distance = 3.144(4) Å, IV = x-1, y, z) with a trigonal planar disposition. The overall pattern of HBs in the (001) planes can be described by a 2D unimodal hexagonal net with point symbol {6^3} with chloride ions and Pyr molecules as three connected nodes and THEO molecules as spacers (Figure 1b). The distance between the different layers is approximately 3.3 Å, similar to that of π-π stacking-based systems, and there is no directional interaction that connects the planes. Interestingly, the HB network formed by PyrH$^+$Cl$^-$ in the codrug (i.e. intramolecular O10-H10···O11, N1$^+$-H1···Cl1$^-$, and O12-H12···Cl1$^-$) resembles that of pure PyrH$^+$Cl$^-$ (CSD code: PYRXCL01; O10···O11, N1$^+$···Cl1$^-$, and O12···Cl1$^-$ distances = 2.598, 3.113 and 3.086 Å, respectively) suggesting that this is the most stable conformation/HB arrangement for this salt.

a)

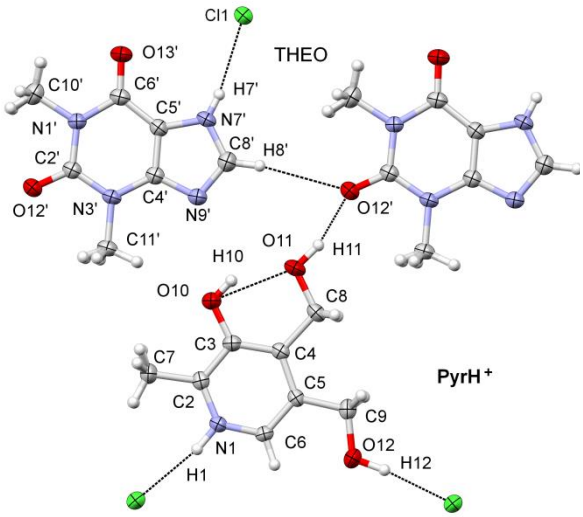

b)

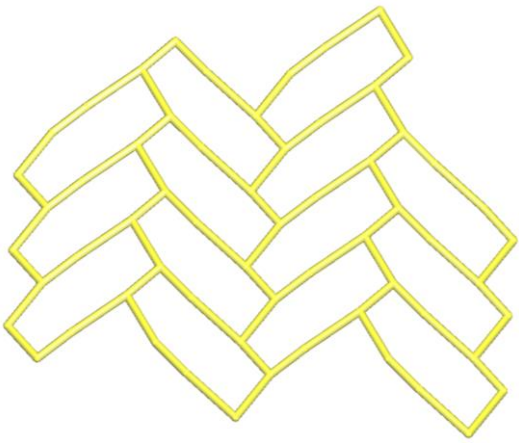

c)

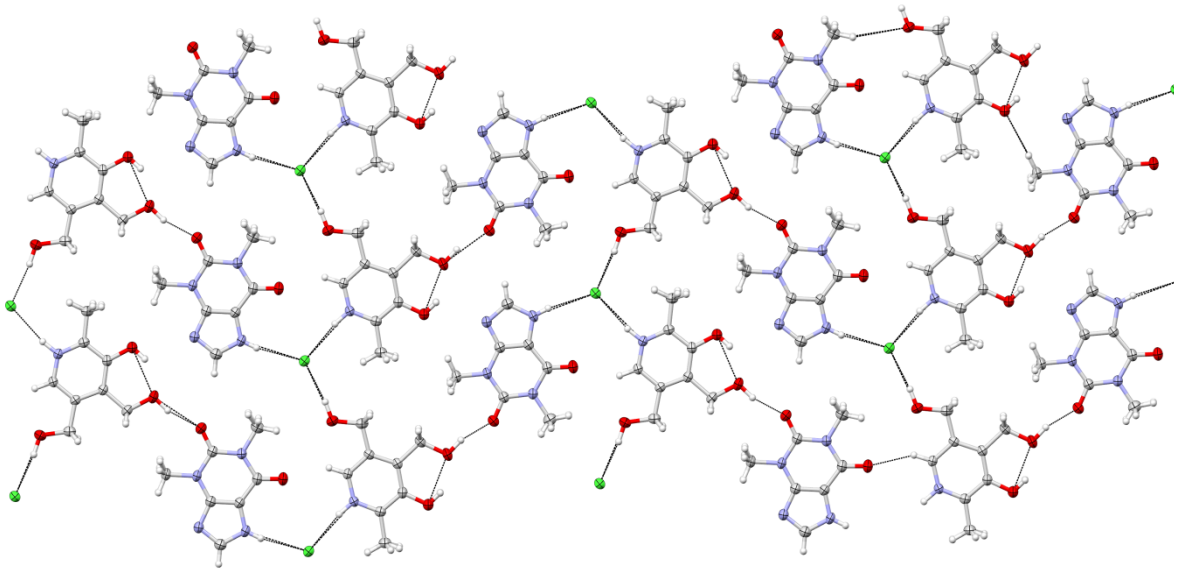

Figure 1. (a) Crystal structure of THEO·PyrH$^+$Cl$^-$ (thermal ellipsoids at 70%), with atom numbering. (b) 2D unimodal hexagonal net formed by intermolecular HB interactions in the (001) planes (see main text). (c) Representation of the structure (thermal ellipsoids at 70%) of the (001) layer. C: gray; H: white; O: red; N: azure; Cl: green.

SSNMR and DFT calculations were effectively combined to address the following points: a) probing the nature of the adduct, i.e. whether neutral (cocrystal) or ionic (salt), b) unravelling the complex HB network and c) to better define the position of H10, i.e. whether pointing toward O11 to form a O10-H10···O11 HB or toward N9' to form a O10-H10···N9' contact. This approach has been successfully applied in the literature, in particular for those cases in which the structure was solved from the XRPD pattern.[61–66] In this context, we demonstrated that it can complete and support a single crystal structure especially when characterized by an extensive and complex HB network. Indeed, SSNMR is well suited to probe the environment of H-bonded atoms by means of dipolar-based 2D experiments.[67] On the other hand, periodic DFT calculations with dispersion correction give a reliable correlation between the position of light atoms (such as hydrogen) and the energy of the system. Furthermore, they support the chemical shift assignment that can often prove challenging because of the strong overlapping as in THEO·PyrH$^+$Cl$^-$, where 5 HB donors (3 OH and 2 NH groups) are present. Thus, 1D (^{1}H MAS, ^{13}C and ^{15}N CPMAS) and 2D experiments (^{1}H DQ MAS, ^{13}C-^{1}H HETCOR, ^{14}N-^{1}H J- and D-HMQC) were acquired. Table 2 lists experimental and computed ^{1}H, ^{13}C and ^{15}N chemical shifts with assignments.

Table 2. Experimental and computed ^{1}H, ^{13}C and ^{15}N chemical shifts with assignments of THEO (experimental only), PyrH$^+$Cl$^-$ (experimental only) and THEO·PyrH$^+$Cl$^-$. The ^{13}C-^{1}H short-range (contact time 2 = 0.4 ms) HETCOR (see Figure S5 in the Supporting Information) was fundamental for the ^{1}H and ^{13}C assignments in THEO·PyrH$^+$Cl$^-$.

# atom	δ ^{1}H (ppm)				type	δ ^{13}C (ppm)				δ ^{15}N (ppm)			
	THEO (exp)	PyrH$^+$Cl$^-$ (exp)	codrug exp	codrug calc		THEO (exp)	PyrH$^+$Cl$^-$ (exp)	codrug exp	codrug calc	THEO (exp)	PyrH$^+$Cl$^-$ (exp)	codrug exp	codrug calc
1		14.6	14.1	13.7							200.0	191.3	189.5
2					C_q		140.9	143.9	145.8				
3					C_q		152.5	154.1	159.9				
4 or 5					C_q		135.6	133.4	138.2				
5 or 4					C_q		135.6	135.2	138.2				
6		7.3	8.1	7.5	CH		124.3	125.9	127.5				
7		2.6	3.3	3.1	CH_3		15.6	16.7	15.2				
8		5.6	5.0	5.6	CH_2		58.2	56.6	64.0				
9		5.6	5.6	5.0	CH_2		61.8	63.5	64.0				
10		10.4	10.4	10.8									
11		5.6	5.3	5.2									
12		5.6	4.9	5.0									
1'										153.4		148.6	163.3
2'					C_q	149.8		152.7	154.6				
3'										111.1		109.4	122.4
4'					C_q	145.1		147.1	150.8				
5'					C_q	104.8		108.9	113.5				
6'					C_q	154.0		152.7	156.3				
7'	14.6		13.8	14.6						161.9		158.4	164.8
8'	7.7		7.5	6.9	CH	139.8		136.7	138.1				

9'										217.8		231.1	239.7
10'	3.4		3.5	3.0	CH_3	29.0		29.4	27.3				
11'	3.4		3.9	3.6	CH_3	29.0		30.9	29.2				

The presence of a single set of resonances in the ^{13}C and ^{15}N CPMAS NMR spectra (Figures 2 and 3, respectively) confirms the existence of one THEO and one $PyrH^+Cl^-$ molecule in the asymmetric unit, in agreement with X-ray diffraction (see above). The lack of signals due to unreacted starting materials accounts for the quantitative achievement of $THEO{\cdot}PyrH^+Cl^-$.

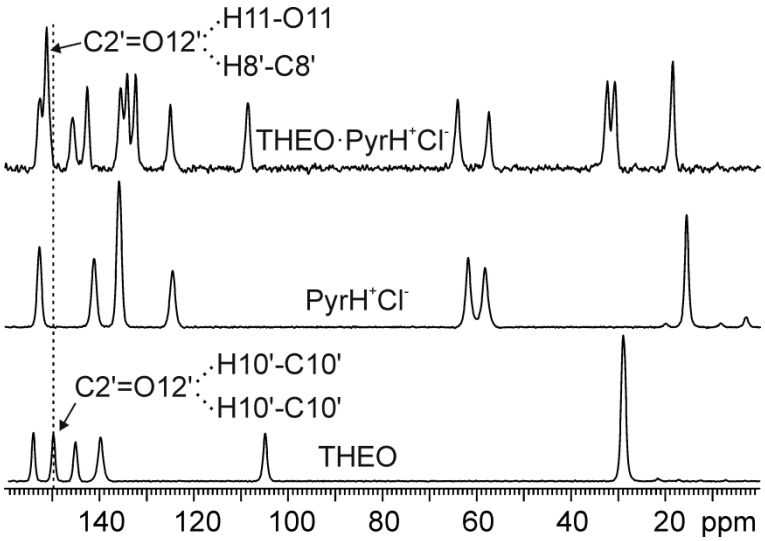

Figure 1. ^{13}C (100.6 MHz) CPMAS (ν_R = 12 kHz) NMR spectra of THEO, $PyrH^+Cl^-$ and $THEO{\cdot}PyrH^+Cl^-$ codrug with relevant assignments.

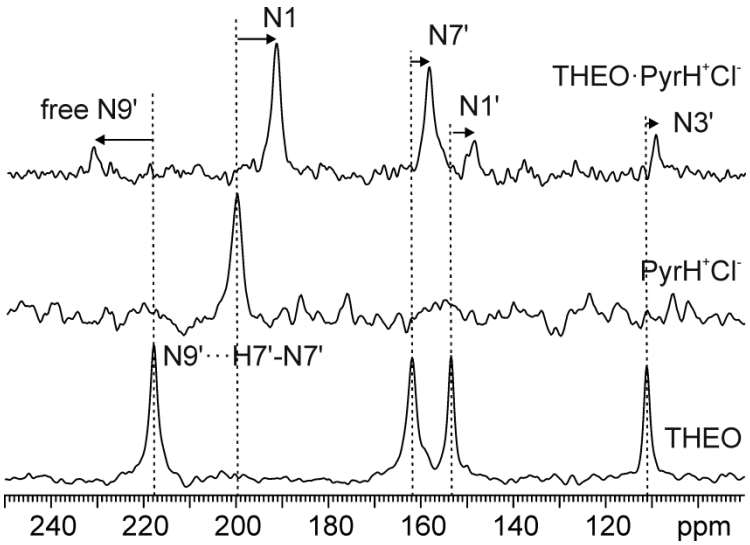

Figure 3. ^{15}N (40.5 MHz) CPMAS (ν_R = 9 kHz) NMR spectra THEO, Pyr and of $THEO{\cdot}PyrH^+Cl^-$ codrug with assignments.

The most relevant ^{13}C shift occurs for the C2'=O12' carbonyl moiety, whose resonance goes from 149.8 (pure THEO) to 152.7 ppm ($THEO{\cdot}PyrH^+Cl^-$). This agrees with the formation of a strong O11-H11···O12' and a weak C8'-H8'···O12' HBs (O11···O12' and C8'···O12' distances = 2.703(5) and 3.593(4) Å, respectively) with respect to the two weak C10'-H10'···O12' contacts (C10'···O12' distances = 3.101 and 3.421 Å) present in pure THEO (form II). On the other hand, since the HB arrangement of $PyrH^+Cl^-$ does not change from pure $PyrH^+Cl^-$ to $THEO{\cdot}PyrH^+Cl^-$, C3, C8 and C9 show only small shifts (around 1.6-1.7 ppm), owing to the codrug formation.

The ^{15}N CPMAS spectrum of THEO·PyrH$^+$Cl$^-$ (Figure 3) provides evidence that N9' is not involved in any interaction and thus H10 points toward O11 to form an intramolecular HB. In pure THEO form II, N9' forms a N7'-H7'···N9' HB (N7'···N9' distance = 2.786 Å) and its resonance falls at 217.8 ppm. Upon cocrystallization, in THEO·PyrH$^+$Cl$^-$ the signal moves toward higher frequencies to 231.1 ppm ($\Delta\delta$ = 13.3 ppm), typical of a free N atom not involved in any interaction. Indeed, it is well known that low-frequency shifts of aromatic nitrogen peaks implies the formation of HB interactions.[68,69]

Figure 4 shows the ^{1}H MAS spectra of both the starting materials (THEO and PyrH$^+$Cl$^-$) and the codrug. The latter is characterized by two signals in the HB region (δ > 10 ppm) at ~ 14.0 and 10.4 ppm (integral ratio 2:1). The former is attributed, thanks to the ^{14}N-^{1}H J- and D-HMQC spectra (see below), to H7' (13.8 ppm) and H1 (14.1 ppm), both involved in strong HBs (N···Cl distances: 3.144 and 3.206 Å, respectively); the latter is due to H10 involved in the intramolecular O10-H10···O11 HB. Clearly, the two remaining OH signals, H11 and H12, fall in an uncommon region for H-bonded atoms. Their assignment at 5.3 and 4.9 ppm, respectively was possible only by combining computational data with ^{1}H DQ MAS and ^{14}N-^{1}H D-HMQC spectra. Interestingly, according to the ^{1}H chemical shift (5.3 ppm) which is known to be diagnostic of the strength of HBs, the O11-H11···O12' HB (O11···O12' distance = 2.703(5) Å), which directly connects the two molecular fragments, is a weak interaction.

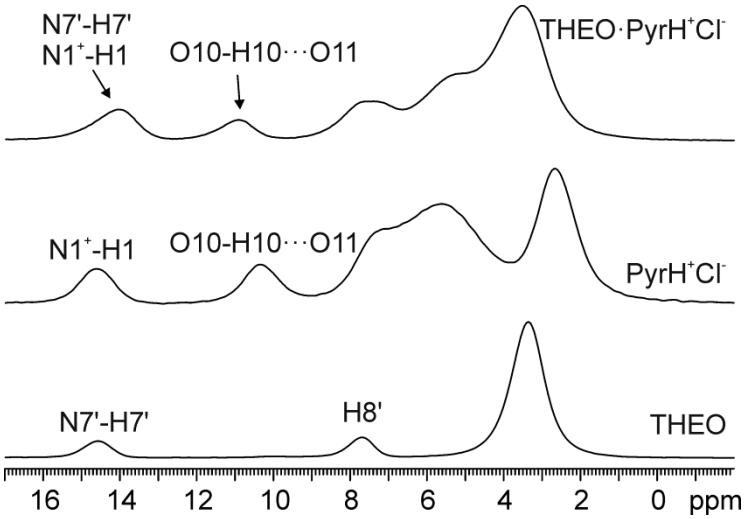

Figure 4. ^{1}H (600.1 MHz) MAS (ν_R = 70 kHz) NMR spectra of THEO, PyrH$^+$Cl$^-$ and THEO·PyrH$^+$Cl$^-$ codrug with relevant assignments.

Figure 5a presents the 2D ^{14}N-^{1}H J-HMQC spectrum. In this experiment, no ^{1}H rf field is applied during t_1 so that the magnetization transfer is driven by a combination of the isotropic part of the J-coupling tensor, which does not vanish with MAS, and the residual dipolar splitting (RDS). The spectrum shows only two correlation peaks, corresponding to covalently bonded N-H atoms (i.e. N1$^+$-H1 and N7'-H7') and allows the determination of their chemical shifts at 14.1 and 13.8 ppm (see below the D-HMQC data for the proper assignment). The lack of a third correlation rules out any possible presence of N9'$^+$-H···O10$^-$ HB. On the other hand, the N1$^+$-H1 correlation confirms the ionic character of the PyrH$^+$Cl$^-$ moiety also in the codrug. Moreover, since there is no proton transfer between THEO and PyrH$^+$Cl$^-$, the codrug can be more properly defined as a drug-drug salt cocrystal.

The D-version of the ^{14}N-^{1}H HMQC experiment (Figure 5b) was performed to observe longer-range N···H proximities. A symmetry-based sequence (SR4) was applied during t_1 to reintroduce the heteronuclear ^{14}N-^{1}H dipolar interactions, usually averaged out by MAS. In this way, signals of both covalently linked N-H and through-space dipolar coupled N···H are observed. The spectrum allows an unambiguous assignment of H1 and H7' at 14.1 and 13.8 ppm, respectively through the correlations of the N1 and N7' resonances. Indeed, N1 gives a correlation also with the signal at 7.5 ppm attributed to H6 while N7' correlates with the peak at 8.1 ppm due to H8'. Moreover, both N1 and N7' show a correlation with a methyl signal (H7 and H11', respectively) in agreement with the proximities highlighted in the X-ray structure. On the other hand, N9' does not present any correlation with H10, confirming the lack of the O-H···N interaction. N-H distances (data obtained from the DFT optimized structure) related to the observed correlations are listed in Table S2.

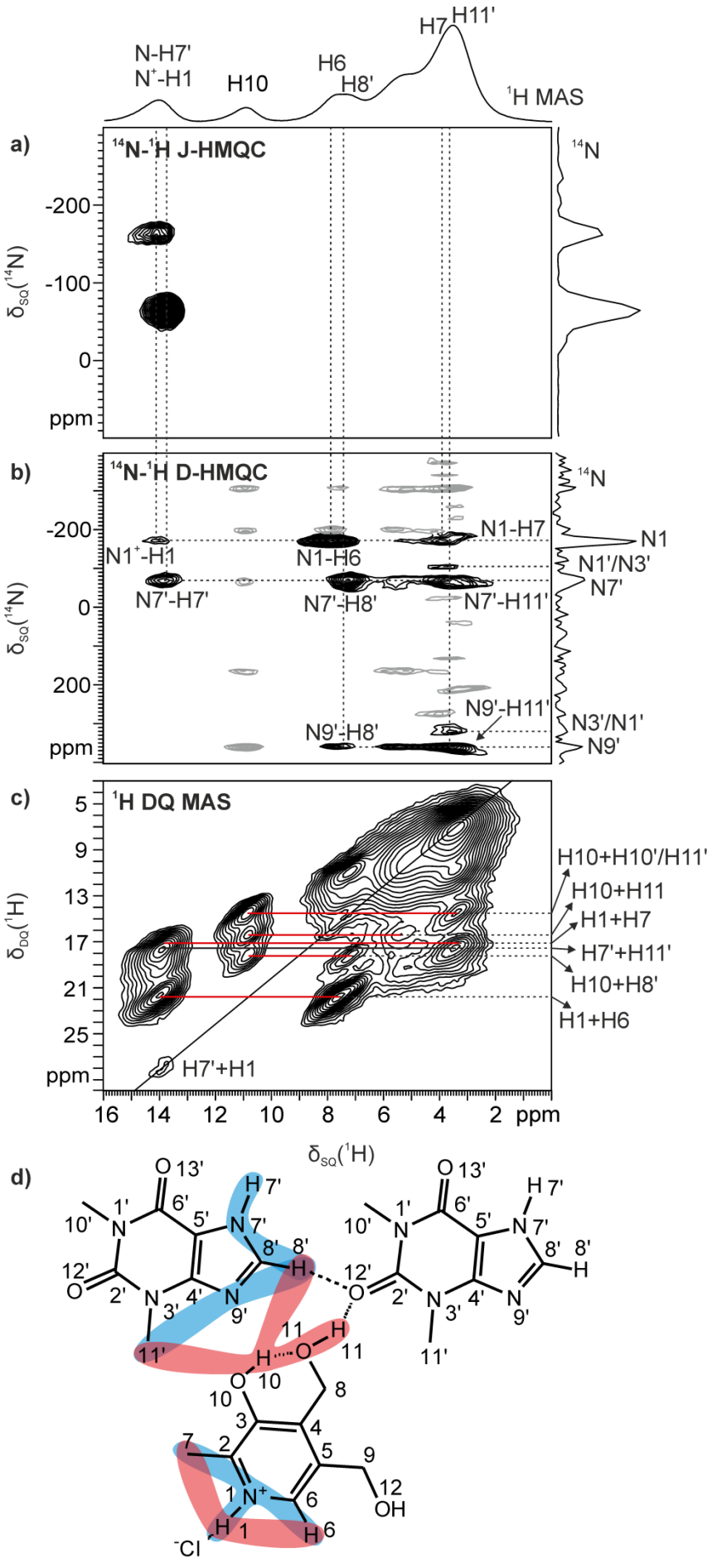
a)
^{14}N-^{1}H J-HMQC
N-H7'
N^{+}-H1
H10
H6
H8'
H7
H11'
^{1}H MAS
^{14}N
-200
-100
0
ppm
$\delta_{SQ}(^{14}N)$
b)
^{14}N-^{1}H D-HMQC
N1^{+}-H1
N1-H6
N1-H7
N7'-H7'
N7'-H8'
N7'-H11'
N9'-H11'
N9'-H8'
N1
N1'/N3'
N7'
N3'/N1'
N9'
200
c)
^{1}H DQ MAS
$\delta_{DQ}(^{1}H)$
5
9
13
17
21
25
H10+H10'/H11'
H10+H11
H1+H7
H7'+H11'
H10+H8'
H1+H6
H7'+H1
16
14
12
10
8
6
4
2
ppm
d)
$\delta_{SQ}(^{1}H)$
O 13'
H 7'
1'
6'
5'
10'
N
N 7'
8' 8'
12'
O
2'
N
3'
4'
N
9'
H
11'
11
H
O
10
8
3
4
7
2
5
9
1 N^{+}
6
12
OH
H 1
H 6
$^{-}$Cl

Figure 5. 2D SSNMR spectra of THEO·PyrH$^+$Cl$^-$. (a) 2D ^{14}N-^{1}H (^{1}H = 600.1 MHz; ^{14}N = 43.4 MHz) J-HMQC (ν_R= 70 kHz) spectrum recorded using $t_{exc} = t_{rec}$=1.49 ms. (b) 2D ^{14}N-^{1}H (^{1}H = 600.1 MHz; ^{14}N = 43.4 MHz) D-HMQC (ν_R= 70 kHz) spectrum recorded using the SR4 recoupling scheme during t_1 with an rf field of 155.8 kHz and $t_{exc} = t_{rec}$ = 0.51 ms. Artifact correlations due to t_1 noise are depicted in gray. (c) 2D ^{1}H (600.1 MHz) DQ MAS (ν_R = 70 kHz) spectrum recorded using one period of BABA recoupling. DQ correlations between nearby hydrogen atoms are highlighted by thick horizontal lines (red for correlations within the layer, black for correlations between different layers). (d) Scheme of the main spatial proximities as found in the ^{14}N-^{1}H D-HMQC (blue) and ^{1}H DQ MAS (red) spectra.

Figure 5c reports the ^{1}H DQ MAS NMR spectrum of THEO·PyrH$^+$Cl$^-$. Such kind of technique is generally used to probe correlations between pairs of through-space dipolar coupled protons employing schemes such as the BAck-to-BAck (BABA) one to recouple the homonuclear ^{1}H-^{1}H dipolar interaction. DQ peaks appear at the sum of the coupled SQ peaks. In the system under study, the spectrum confirms the assignment of NH protons and allows assigning part of the remaining signals belonging to OH groups. The whole list of correlations is reported in Table S3 in the Supporting Information, while the most important results are depicted in Figure 5d and can be summarized as follows:

- there are intermolecular proximities between H7' (13.8 ppm) and H1 (14.1 ppm) across the Cl$^-$ involved in 3 HBs in trigonal planar disposition (DQ peak at 27.9 ppm) and between H7' (13.8 ppm) and H11' (3.9 ppm) belonging to a molecule of a backward layer (black correlation line in Figure 5c);
- H1 (14.1 ppm) presents two correlations due to intramolecular proximities with H7 (3.3 ppm) and H6 (8.1 ppm);
- H10 (10.4 ppm) correlates with H11' and H10' (3.9 and 3.5 ppm, respectively), H8' (7.5 ppm) and allows the assignment of H11 (5.3 ppm) through the DQ peak at 15.7 ppm.

All the observed correlations perfectly agree with the optimized structure (see below) confirming the correct position of the N-H and O-H hydrogen atoms.

Owing to the complex HB network present in the codrug and to the impossibility of an unambiguous ^{1}H assignment of H12, the X-ray structure was optimized by means of periodic DFT calculations (Quantum Espresso v.5.1.2) with the GGA functional PW86PBE and the inclusion of the exchange-hole dipole moment (XDM) dispersion correction method for the accurate modeling of the HB interaction. The hydrogen atom positions within the HB network refined by SSNMR analysis agree with the optimized structure (Figure 6). To verify the reliability of the optimization, the chemical shifts were computed by the well-known GIPAW method[58,70] and compared with the experimental ones (Table 2). Despite the intrinsic difficulty in modeling N-H hydrogen bonds[71] or in pinpointing O-H,[72,73] experimental and computed values show an excellent agreement (^{1}H RMSD = 0.5 ppm; ^{13}C RMSD = 3.5 ppm). The ^{1}H assignment of H7', H1, H10 and H11 was confirmed and it was possible to attribute the signal at 4.9 ppm (strongly overlapped with the aromatic resonances) to H12.

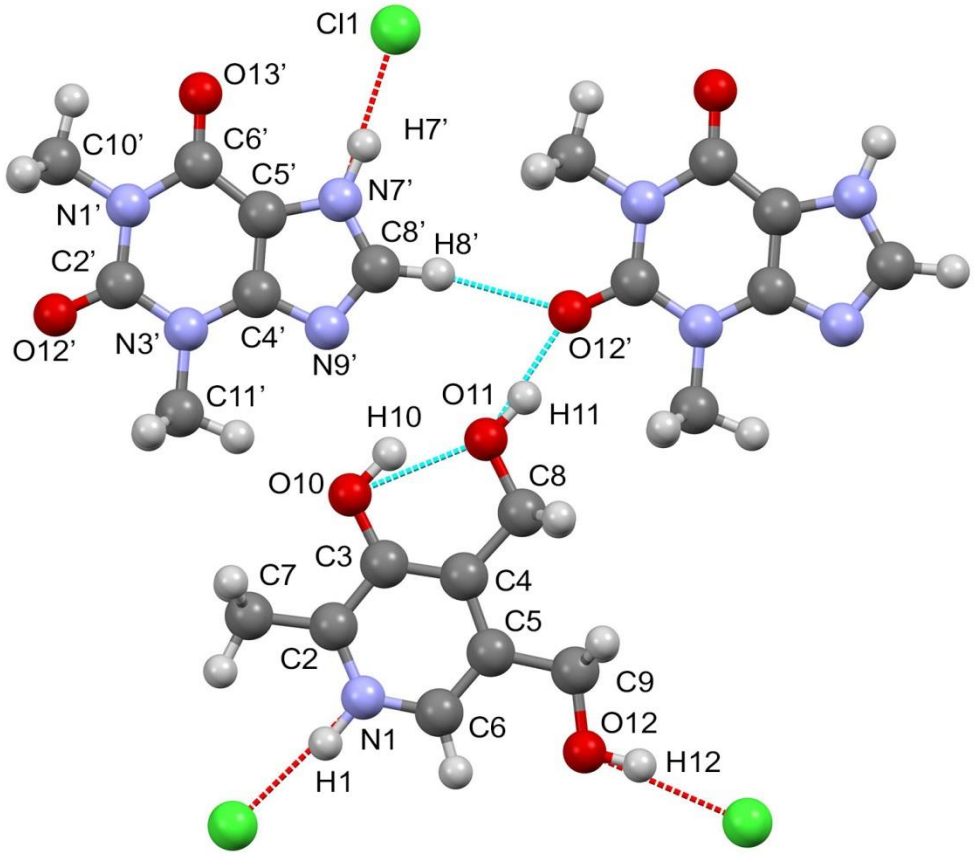

Figure 6. Quantum Espresso optimized structure of THEO·PyrH$^+$Cl$^-$, with atom numbering.

THEO·PyrH$^+$Cl$^-$ was also analyzed by means of DSC and TGA to evaluate its thermal behavior with respect to pure THEO and PyrH$^+$Cl$^-$. All thermograms are reported in Figures S6-S8 in the Supporting Information. The DSC of the codrug (Figure S6) shows two endothermic events at 205°C (peak point; onset T: 200°C) and 230°C (peak point; onset T: 227°C). The former represents the melting point of the codrug, which is also associated to the decomposition of PyrH$^+$Cl$^-$; the latter is attributed to THEO melting and subsequently decomposing. Thus, since the melting/decomposition points of pure THEO and PyrH$^+$Cl$^-$ are 273°C and 214°C (peak points), cocrystallization appears to lead to a slight decrease of the thermal stability of both components.

Conclusions

We reported on the cocrystallization of the THEO·PyrH$^+$Cl$^-$ codrug formed by two APIs, which could turn out to be interesting because they are usually administered in co-therapy. A combined experimental and computational investigation of the codrug by means of SCXRD, SSNMR and DFT calculations was performed to unravel the complex network of HB interactions. The two molecular fragments are connected by two weak HBs, namely O11-H11···O12' and C8'-H8'···O12', and by three interactions which involve the Cl$^-$ ion (N7'-H7'···Cl1$^-$, O12-H12···Cl1$^-$ and N1$^+$-H1···Cl1$^-$) with a trigonal planar disposition.

This represents an interesting model system since characterized by 3 OH and 2 NH hydrogen atoms (5 HB donors) whose positions were poorly defined by single crystal X-ray data. Several advanced 2D SSNMR spectra such as ^{1}H DQ MAS, ^{13}C-^{1}H HETCOR, ^{14}N-^{1}H J- and D-HMQC were acquired, taking advantage of the resolution and sensitivity improvement provided by indirect detection pulse sequences and very fast MAS at 70 kHz. These experiments, supported and completed by DFT calculations, were fundamental to allow an unambiguous assignment of the signals in the ^{1}H MAS spectrum and to accurately determine the position of hydrogen atoms and thus to elucidate the complex HB network. Furthermore, they were fundamental to define the ionic character of the drug-drug cocrystal, which can be more properly defined as a drug-drug salt cocrystal.

Associated content

Supporting Information

The Supporting Information is available free of charge on the ACS Publications website.

Table of the XRD bond lengths and angles, list of the correlations found in the ^{14}N-^{1}H D-HMQC and ^{1}H DQ MAS spectra, Raman spectra, PXRD patterns, XRD asymmetric unit cell, ^{13}C-^{1}H double CP NMR spectrum, DSC and TGS curves, detailed information on solid-state NMR experimental part.

Acknowledgments

The authors are indebted with Jeol Company for helpful technical assistance and cooperation. F.R. thanks Jeol (Italia) S.p.A. for a Ph.D. scholarship.

References

(1) Wan, X.; Ma, P.; Zhang, X. A Promising Choice in Hypertension Treatment: Fixed-Dose Combinations. *Asian J. Pharm. Sci.* **2014**, *9* (1), 1–7.

(2) Institute of Medicine. *Preventing Medication Errors*; Philip Aspden, Julie Wolcott, J. Lyle Bootman, Linda R. Cronenwett, Series Eds.; The National Academies Press: Washington, DC, 2007.

(3) Aitken, M.; Valkova, S. Avoidable Costs in U.S. Healthcare: The $200 Billion Opportunity from Using Medicines More Responsibly. *Report by the IMS Institute for Healthcare Informatics*. 2013.

(4) Aitipamula, S.; Chow, P. S.; Tan, R. B. H. Trimorphs of a Pharmaceutical Cocrystal Involving Two Active Pharmaceutical Ingredients: Potential Relevance to Combination Drugs. *CrystEngComm* **2009**, *11* (9), 1823–1827.

(5) Cheney, M. L.; Weyna, D. R.; Shan, N.; Hanna, M.; Wojtas, L.; Zaworotko, M. J. Coformer Selection in Pharmaceutical Cocrystal Development: A Case Study of a Meloxicam Aspirin Cocrystal That Exhibits Enhanced Solubility and Pharmacokinetics. *J. Pharm. Sci.* **2011**, *100* (6), 2172–2181.

(6) Sanphui, P.; Goud, N. R.; Khandavilli, U. B. R.; Nangia, A. Fast Dissolving Curcumin Cocrystals. *Cryst. Growth Des.* **2011**, *11* (9), 4135–4145.

(7) Lu, J.; Rohani, S. Synthesis and Preliminary Characterization of Sulfamethazine-Theophylline Co-Crystal. *J. Pharm. Sci.* **2010**, *99* (9), 4042–4047.

(8) Jiang, L.; Huang, Y.; Zhang, Q.; He, H.; Xu, Y.; Mei, X. Preparation and Solid-State Characterization of Dapsone Drug–Drug Co-Crystals. *Cryst. Growth Des.* **2014**, *14* (9), 4562–4573.

(9) Thipparaboina, R.; Kumar, D.; Chavan, R. B.; Shastri, N. R. Multidrug Co-Crystals: Towards the Development of Effective Therapeutic Hybrids. *Drug Discov. Today* **2016**, *21* (3), 481–490.

(10) Nakao, S.; Fujii, S.; Sakaki, T.; Tomita, K.-I. The Crystal and Molecular Structure of the 2:1 Molecular Complex of Theophylline with Phenobarbital. *Acta Crystallogr. B* **1977**, *33* (5), 1373–1378.

(11) Zaitu, S.; Miwa, Y.; Taga, T. A 2:1 Molecular Complex of Theophylline and 5-Fluorouracil as the Monohydrate. *Acta Crystallogr. C* **1995**, *51* (9), 1857–1859.

(12) Aitipamula, S.; Chow, P. S.; Tan, R. B. H. Ethenzamide–gentisic Acid–acetic Acid (2/1/1). *Acta Crystallogr. Sect. E Struct. Rep. Online* **2010**, *66* (5), o1045–o1046.

(13) Bhatt, P. M.; Azim, Y.; Thakur, T. S.; Desiraju, G. R. Co-Crystals of the Anti-HIV Drugs Lamivudine and Zidovudine. *Cryst. Growth Des.* **2009**, *9* (2), 951–957.

(14) Bordignon, S.; Cerreia Vioglio, P.; Priola, E.; Voinovich, D.; Gobetto, R.; Nishiyama, Y.; Chierotti, M. R. Engineering Codrug Solid Forms: Mechanochemical Synthesis of an Indomethacin–Caffeine System. *Cryst. Growth Des.* **2017**, *17* (11), 5744–5752.

(15) Press Announcements > FDA approves new drug to treat heart failure https://www.fda.gov/newsevents/newsroom/pressannouncements/ucm453845.htm (accessed Nov 16, 2017).

(16) Wang, J.-R.; Yu, Q.; Dai, W.; Mei, X. Drug–drug Co-Crystallization Presents a New Opportunity for the Development of Stable Vitamins. *Chem. Commun.* **2016**, *52* (17), 3572–3575.

(17) Nainar, S.; Rajiah, K.; Angamuthu, S.; Prabakaran, D.; Kasibhatta, R. Biopharmaceutical Classification System in Invitro/ In-Vivo Correlation: Concept and Development Strategies in Drug Delivery. *Trop. J. Pharm. Res.* **2012**, *11* (2), 319–329.

(18) Brouwers, J.; Ingels, F.; Tack, J.; Augustijns, P. Determination of Intraluminal Theophylline Concentrations after Oral Intake of an Immediate-and a Slow-Release Dosage Form. *J. Pharm. Pharmacol.* **2005**, *57* (8), 987–995.
(19) Pinnamraju Durga Nithya, Sajja Brahmani, Alapati Sriram, Nutalapati Prasanna Jaya Krishna, Poluri Koteswari, Puttagunta Srinivasa Babu. Formulation and Evaluation of Theophylline Controlled Release Matrix Tablets by Using Natural Gums. *Int. J. Pharm. Sci. Rev. Res.* **2014**, *27* (1), 183.
(20) Paloucek, F. P.; Rodvold, K. A. Evaluation of Theophylline Overdoses and Toxicities. *Ann. Emerg. Med.* **1988**, *17* (2), 135–144.
(21) Glenn, G. M.; Krober, M. S.; Kelly, P.; McCarty, J.; Weir, M. Pyridoxine as Therapy in Theophylline-Induced Seizures. *Vet. Hum. Toxicol.* **1995**, *37* (4), 342–345.
(22) Ubbink, J. B.; Vermaak, W. J. H.; Delport, R.; Serfontein, W. J.; Bartel, P. The Relationship between Vitamin B6 Metabolism, Asthma, and Theophylline Therapy. *Ann. N. Y. Acad. Sci.* **1990**, *585* (1), 285–294.
(23) Delport, R.; Ubbink, J. B.; Serfontein, W. J.; Becker, P. J.; Walters, L. Vitamin B6 Nutritional Status in Asthma: The Effect of Theophylline Therapy on Plasma Pyridoxal-5'-Phosphate and Pyridoxal Levels. *Int. J. Vitam. Nutr. Res. Int. Z. Vitam.- Ernahrungsforschung J. Int. Vitaminol. Nutr.* **1988**, *58* (1), 67–72.
(24) Naqvi, A. A.; Bhattacharyya, G. C. Crystal Data for Anhydrous Theophylline. *J. Appl. Crystallogr.* **1981**, *14* (6), 464–464.
(25) Zhang, S.; Fischer, A. A Monoclinic Polymorph of Theophylline. *Acta Crystallogr. Sect. E Struct. Rep. Online* **2011**, *67* (12), o3357–o3357.
(26) Pinon, A. C.; Rossini, A. J.; Widdifield, C. M.; Gajan, D.; Emsley, L. Polymorphs of Theophylline Characterized by DNP Enhanced Solid-State NMR. *Mol. Pharm.* **2015**, *12* (11), 4146–4153.
(27) Dyulgerov, V. M.; Dimowa, L. T.; Kossev, K.; Nikolova, R. P.; Shivachev, B. L. Solvothermal Synthesis of Theophylline and N,N'-(Ethane-1,2-Diyl)Diformamide Cocrystals from DMF Decomposition and N-Formylation Trough Catalytic Effect of 3-Carboxyphenylboronic Acid and Cadmium Acetate. *Bulg. Chem. Commun.* **2015**, *47* (1), 311.
(28) Sutor, D. J. The Structures of the Pyrimidines and Purines. VI. The Crystal Structure of Theophylline. *Acta Crystallogr.* **1958**, *11* (2), 83–87.
(29) Fucke, K.; McIntyre, G. J.; Wilkinson, C.; Henry, M.; Howard, J. A. K.; Steed, J. W. New Insights into an Old Molecule: Interaction Energies of Theophylline Crystal Forms. *Cryst. Growth Des.* **2012**, *12* (3), 1395–1401.
(30) Surov, A. O.; Voronin, A. P.; Manin, A. N.; Manin, N. G.; Kuzmina, L. G.; Churakov, A. V.; Perlovich, G. L. Pharmaceutical Cocrystals of Diflunisal and Diclofenac with Theophylline. *Mol. Pharm.* **2014**, *11* (10), 3707–3715.
(31) Uldry, A.-C.; Griffin, J. M.; Yates, J. R.; Pérez-Torralba, M.; Santa María, M. D.; Webber, A. L.; Beaumont, M. L. L.; Samoson, A.; Claramunt, R. M.; Pickard, C. J.; et al. Quantifying Weak Hydrogen Bonding in Uracil and 4-Cyano-4'-Ethynylbiphenyl: A Combined Computational and Experimental Investigation of NMR Chemical Shifts in the Solid State. *J. Am. Chem. Soc.* **2008**, *130* (3), 945–954.
(32) Brown, S. P. Hydrogen Bonding in Crystalline Organic Solids. *In NMR Crystallography; Harris RK, Wasylishen R., Duer MJ, Eds*. John Wiley & Sons Ltd, Chichester (UK). 2009, pp 321–339.
(33) Hong, M.; Fritzsching, K. J.; Williams, J. K. Hydrogen-Bonding Partner of the Proton-Conducting Histidine in the Influenza M2 Proton Channel Revealed From 1H Chemical Shifts. *J. Am. Chem. Soc.* **2012**, *134* (36), 14753–14755.
(34) Chierotti, M. R.; Gobetto, R. Solid-State NMR Studies of Weak Interactions in Supramolecular Systems. *Chem. Commun.* **2008**, *0* (14), 1621–1634.
(35) Stevens, J. S.; Byard, S. J.; Seaton, C. C.; Sadiq, G.; Davey, R. J.; Schroeder, S. L. M. Proton Transfer and Hydrogen Bonding in the Organic Solid State: A Combined XRD/XPS/SsNMR Study of 17 Organic Acid–base Complexes. *Phys. Chem. Chem. Phys.* **2013**, *16* (3), 1150–1160.
(36) Gobetto, R.; Nervi, C.; Chierotti, M. R.; Braga, D.; Maini, L.; Grepioni, F.; Harris, R. K.; Hodgkinson, P. Hydrogen Bonding and Dynamic Behaviour in Crystals and Polymorphs of Dicarboxylic-Diamine Adducts: A Comparison between NMR Parameters and X-Ray Diffraction Studies. *Chem.- Eur. J.* **2005**, *11* (24), 7461–7471.

(37) Chierotti, M. R.; Gobetto, R.; Nervi, C.; Bacchi, A.; Pelagatti, P.; Colombo, V.; Sironi, A. Probing Hydrogen Bond Networks in Half-Sandwich Ru(II) Building Blocks by a Combined 1H DQ CRAMPS Solid-State NMR, XRPD, and DFT Approach. *Inorg. Chem.* **2014**, *53* (1), 139–146.
(38) Bradley, J. P.; Velaga, S. P.; Antzutkin, O. N.; Brown, S. P. Probing Intermolecular Crystal Packing in γ-Indomethacin by High-Resolution 1H Solid-State NMR Spectroscopy. *Cryst. Growth Des.* **2011**, *11* (8), 3463–3471.
(39) Spinelli, F.; Dichiarante, E.; Curzi, M.; Giaffreda, S. L.; Chierotti, M. R.; Gobetto, R.; Rossi, F.; Chelazzi, L.; Braga, D.; Grepioni, F. Molecular Salts of the Antidepressant Venlafaxine: An Effective Route to Solubility Properties Modifications. *Cryst. Growth Des.* **2017**.
(40) Rajput, L.; Banik, M.; Yarava, J. R.; Joseph, S.; Pandey, M. K.; Nishiyama, Y.; Desiraju, G. R. Exploring the Salt–cocrystal Continuum with Solid-State NMR Using Natural-Abundance Samples: Implications for Crystal Engineering. *IUCrJ* **2017**, *4* (4), 466–475.
(41) Cavadini, S.; Antonijevic, S.; Lupulescu, A.; Bodenhausen, G. Indirect Detection of Nitrogen-14 in Solids via Protons by Nuclear Magnetic Resonance Spectroscopy. *J. Magn. Reson.* **2006**, *182* (1), 168–172.
(42) Nishiyama, Y.; Endo, Y.; Nemoto, T.; Utsumi, H.; Yamauchi, K.; Hioka, K.; Asakura, T. Very Fast Magic Angle Spinning 1H-14N 2D Solid-State NMR: Sub-Micro-Liter Sample Data Collection in a Few Minutes. *J. Magn. Reson.* **2011**, *208* (1), 44–48.
(43) Perras, F. A.; Bryce, D. L. Residual Dipolar Coupling between Quadrupolar Nuclei under Magic-Angle Spinning and Double-Rotation Conditions. *J. Magn. Reson.* **2011**, *213* (1), 82–89.
(44) Gan, Z.; Amoureux, J. P.; Trébosc, J. Proton-Detected 14N MAS NMR Using Homonuclear Decoupled Rotary Resonance. *Chem. Phys. Lett.* **2007**, *435* (1), 163–169.
(45) Cavadini, S.; Abraham, A.; Bodenhausen, G. Proton-Detected Nitrogen-14 NMR by Recoupling of Heteronuclear Dipolar Interactions Using Symmetry-Based Sequences. *Chem. Phys. Lett.* **2007**, *445* (1), 1–5.
(46) Pindelska, E.; Sokal, A.; Szeleszczuk, L.; Pisklak, D. M.; Kolodziejski, W. Solid-State NMR Studies of Theophylline Co-Crystals with Dicarboxylic Acids. *J. Pharm. Biomed. Anal.* **2014**, *100* (Supplement C), 322–328.
(47) *Agilent Technologies, CrysAlisProSoftare System*; Agilent Technologies U K Ltd.: Oxford, U.K, 2012.
(48) Sheldrick, G. M. *SHELX97: Program for Crystal Structure Solution and Refinement*; University of Göttingen: Göttingen, Germany, 2004.
(49) Blatov, V. A.; Shevchenko, A. P.; Proserpio, D. M. Applied Topological Analysis of Crystal Structures with the Program Package ToposPro. *Cryst. Growth Des.* **2014**, *14* (7), 3576–3586.
(50) Etter, M. C.; MacDonald, J. C.; Bernstein, J. Graph-Set Analysis of Hydrogen-Bond Patterns in Organic Crystals. *Acta Crystallogr. B* **1990**, *46 (Pt 2)*, 256–262.
(51) Macrae, C. F.; Edgington, P. R.; McCabe, P.; Pidcock, E.; Shields, G. P.; Taylor, R.; Towler, M.; Streek, J. van de. Mercury: Visualization and Analysis of Crystal Structures. *J. Appl. Crystallogr.* **2006**, *39* (3), 453–457.
(52) Potrzebowski, M. J.; Tekely, P.; Dusausoy, Y. Comment to 13C-NMR Studies of α and γ Polymorphs of Glycine. *Solid State Nucl. Magn. Reson.* **1998**, *11* (3), 253–257.
(53) Ye, C.; Fu, R.; Hu, J.; Hou, L.; Ding, S. Carbon-13 Chemical Shift Anisotropies of Solid Amino Acids. *Magn. Reson. Chem.* **1993**, *31* (8), 699–704.
(54) Paolo Giannozzi et al. QUANTUM ESPRESSO: A Modular and Open-Source Software Project for Quantum Simulations of Materials. *J. Phys. Condens. Matter* **2009**, *21* (39), 395502.
(55) Perdew, J. P.; Burke, K.; Ernzerhof, M. Generalized Gradient Approximation Made Simple. *Phys. Rev. Lett.* **1996**, *77* (18), 3865–3868.
(56) Otero-de-la-Roza, A.; Johnson, E. R.; DiLabio, G. A. Halogen Bonding from Dispersion-Corrected Density-Functional Theory: The Role of Delocalization Error. *J. Chem. Theory Comput.* **2014**, *10* (12), 5436–5447.
(57) Kresse, G.; Joubert, D. From Ultrasoft Pseudopotentials to the Projector Augmented-Wave Method. *Phys. Rev. B* **1999**, *59* (3), 1758–1775.
(58) Pickard, C. J.; Mauri, F. All-Electron Magnetic Response with Pseudopotentials: NMR Chemical Shifts. *Phys. Rev. B* **2001**, *63* (24), 245101.

(59) Monkhorst, H. J.; Pack, J. D. Special Points for Brillouin-Zone Integrations. *Phys. Rev. B* **1976**, *13* (12), 5188–5192.
(60) Desiraju, G. R.; Steiner, T. The Weak Hydrogen Bond: In Structural Chemistry and Biology. In *The Weak Hydrogen Bond: In Structural Chemistry and Biology*; Eds. Oxford University Press: New York, 2006; pp 352–355.
(61) Többens, D. M.; Glinneman, J.; Chierotti, M. R.; Streek, J. van de; Sheptyakov, D. On the High-Temperature Phase of Barbituric Acid. *CrystEngComm* **2012**, *14* (9), 3046–3055.
(62) Gumbert, S. D.; Koerbitzer, M.; Alig, E.; Schmidt, M. U.; Chierotti, M. R.; Gobetto, R.; Li, X.; van de Streek, J. Crystal Structure and Tautomerism of Pigment Yellow 138 Determined by X-Ray Powder Diffraction and Solid-State NMR. *Dyes Pigments* **2016**, *131*, 364–372.
(63) Watts, A. E.; Maruyoshi, K.; Hughes, C. E.; Brown, S. P.; Harris, K. D. M. Combining the Advantages of Powder X-Ray Diffraction and NMR Crystallography in Structure Determination of the Pharmaceutical Material Cimetidine Hydrochloride. *Cryst. Growth Des.* **2016**, *16* (4), 1798–1804.
(64) Paluch, P.; Pawlak, T.; Oszajca, M.; Lasocha, W.; Potrzebowski, M. J. Fine Refinement of Solid State Structure of Racemic Form of Phospho-Tyrosine Employing NMR Crystallography Approach. *Solid State Nucl. Magn. Reson.* **2015**, *65*, 2–11.
(65) Dudenko, D. V.; Williams, P. A.; Hughes, C. E.; Antzutkin, O. N.; Velaga, S. P.; Brown, S. P.; Harris, K. D. M. Exploiting the Synergy of Powder X-Ray Diffraction and Solid-State NMR Spectroscopy in Structure Determination of Organic Molecular Solids. *J. Phys. Chem. C* **2013**, *117* (23), 12258–12265.
(66) Bērziņš, A.; Hodgkinson, P. Solid-State NMR and Computational Investigation of Solvent Molecule Arrangement and Dynamics in Isostructural Solvates of Droperidol. *Solid State Nucl. Magn. Reson.* **2015**, *65*, 12–20.
(67) Chierotti, M. R.; Gobetto, R. NMR Crystallography: The Use of Dipolar Interactions in Polymorph and Co-Crystal Investigation. *Crystengcomm* **2013**, *15* (43), 8599–8612.
(68) Vioglio, P. C.; Chierotti, M. R.; Gobetto, R. Solid-State Nuclear Magnetic Resonance as a Tool for Investigating the Halogen Bond. *CrystEngComm* **2016**, *18* (48), 9173–9184.
(69) Cerreia Vioglio, P.; Chierotti, M. R.; Gobetto, R. Pharmaceutical Aspects of Salt and Cocrystal Forms of APIs and Characterization Challenges. *Adv. Drug Deliv. Rev.* **2017**, *117* (Supplement C), 86–110.
(70) Franco, F.; Baricco, M.; Chierotti, M. R.; Gobetto, R.; Nervi, C. Coupling Solid-State NMR with GIPAW Ab Initio Calculations in Metal Hydrides and Borohydrides. *J. Phys. Chem. C* **2013**, *117* (19), 9991–9998.
(71) Kerr, H. E.; Softley, L. K.; Suresh, K.; Nangia, A.; Hodgkinson, P.; Evans, I. R. A Furosemide–isonicotinamide Cocrystal: An Investigation of Properties and Extensive Structural Disorder. *CrystEngComm* **2015**, *17* (35), 6707–6715.
(72) Harris, R. K.; Hodgkinson, P.; Zorin, V.; Dumez, J.-N.; Elena-Herrmann, B.; Emsley, L.; Salager, E.; Stein, R. S. Computation and NMR Crystallography of Terbutaline Sulfate. *Magn. Reson. Chem.* **2010**, *48* (S1), S103–S112.
(73) Kibalchenko, M.; Lee, D.; Shao, L.; Payne, M. C.; Titman, J. J.; Yates, J. R. Distinguishing Hydrogen Bonding Networks in α-d-Galactose Using NMR Experiments and First Principles Calculations. *Chem. Phys. Lett.* **2010**, *498* (4), 270–276.

FOR TABLE OF CONTENTS ONLY

UNRAVELING THE HYDROGEN BOND NETWORK IN A THEOPHYLLINE-PYRIDOXINE SALT COCRYSTAL BY A COMBINED X-RAY DIFFRACTION, SOLID-STATE NMR AND COMPUTATIONAL APPROACH

Federica Rossi, Paolo Cerreia Vioglio, Simone Bordignon, Valeria Giorgio, Carlo Nervi, Emanuele Priola, Roberto Gobetto, Koji Yazawa, Michele R. Chierotti*

SYNOPSIS

We report on the synthesis of a codrug between theophylline and pyridoxine·HCl. The codrug was characterized by a combined experimental and computational investigation by means of SCXRD, SSNMR and DFT calculations. The complex network of hydrogen bond interactions was unraveled by defining the position of hydrogen atoms, as well as the ionic character of the codrug.